INSTITUTE OF PHYSICS PUBLISHING SUPERCONDUCTOR SCIENCE AND TECHNOLOGY

Supercond. Sci. Technol. **19** (2006) S590–S600 doi:10.1088/0953-2048/19/7/S33

Fabrication and characterization of thin-wall YBCO single-domain samples

X Chaud[1,6], D Bourgault[1,2], D Chateigner[3], P Diko[4], L Porcar[1,5], A Villaume[1,2], A Sulpice[1,5] and R Tournier[1,2]

[1] CNRS/CRETA, BP 166, 38042 Grenoble Cedex 09, France
[2] CNRS/LdC, BP 166, 38042 Grenoble Cedex 09, France
[3] CRISMAT-ENSICAEN, 6 Boulevard Maréchal Juin, 14050 Caen, France
[4] Institute of Experimental Physics, Slovak Academy of Sciences, Watsonova 47, 043 53 Kosice, Slovakia
[5] CNRS/CRTBT, BP 166, 38042 Grenoble Cedex 09, France

E-mail: xavier.chaud@grenoble.cnrs.fr

Received 6 January 2006, in final form 3 March 2006
Published 11 May 2006
Online at stacks.iop.org/SUST/19/S590

Abstract

Thin-wall geometry implies a regular network of holes in a bulk, centimetric sample so that its effective thickness can be considered to be smaller than 1.5 mm. Thin-wall geometry offers a significant potential for helping the oxygenation process, mechanical reinforcement and thermal stabilization. Thin-wall geometry was obtained by drilling holes in slightly sintered pellets or by pressing pellets with embedded needles. The growth of a single domain, up to 50 mm in diameter, on such thin-wall geometry pellets was confirmed, despite the presence of many-hole patterns, by *in situ* high-temperature video monitoring. A significant decrease of porosity and cracks is observed, associated with the reduction of diffusion paths produced by thin-wall geometry. The improvement of the material quality is established by a significant increase (about 40%) of the magnetic trapped field in thin-wall samples.

(Some figures in this article are in colour only in the electronic version)

M This article features online multimedia enhancements

1. Introduction

The preparation of $YBa_2Cu_3O_{7-\delta}$ (Y123) single-domain samples by top-seeding melt-growth (TSMG) techniques yields high-temperature superconducting materials highly suitable for practical applications at 77 K. Their use is usually devoted to devices for which no equivalent can be obtained by conventional technologies. This is the case for autostable superconducting bearings [1], fault current limiters [2], and superconducting trapped-field magnets [3]. They can also lead to very compact and efficient cryogenic motors and generators [4].

Y123 single-domain samples are practically large single crystals with defects such as secondary phase particles of Y_2BaCuO_5 (Y211), pores, cracks, and slight crystal misalignment. They are routinely produced nowadays up to 4 cm. Larger sizes up to 10 cm [5] and even up to 14 cm [6] have already been grown. Rare earths such as samarium, neodymium, or gadolinium can be substituted for yttrium [7] and yield RE123 single domains with improved performances.

For applications such as trapped field the properties can be enhanced by fine added pinning centres, e.g. additional non-superconducting phases, and by the size of the current loops in the sample, e.g. the size of the single domain [8]. However, defects resulting in detriment to the superconducting properties become more difficult to avoid with increasing single-domain size. The added, fine phases are usually inhomogeneously distributed due to the pushing–trapping phenomenon where small particles are pushed by the advancing growth front. This inhomogeneity reduces the critical currents as well as the mechanical properties. Cracks are then seen to develop

[6] Author to whom any correspondence should be addressed.

between areas of different secondary phase contents [9]. Radial cracks also occur during cooling because of enhanced thermal gradient on large pellets [10]. These cracks may be limited by using medium range secondary particles (around 2 μm) and by a careful temperature control during large pellet cooling.

Some other cracks remain in the first and second cleavage planes of Y123, a/c-(100) and a/b-(001) planes, respectively. The a/c-cracks hinder the current flow in the a/b-planes, and therefore influence the size of the current loop, i.e. the levitation forces and the trapped field. The a/b-cracks impede the current flow along the c-axis in certain current-limiting applications [11, 12] and influence those applications requiring the current to flow in the a/b-plane by the overall degradation of the mechanical properties. The existence of these cracks partly explains why properties measured on large (cm) samples are inferior to what one would expect by extrapolating current-related properties measured on small (mm) samples (e.g. [13]).

A peculiarity of the single-domain fabrication is the necessity to perform an oxygen-annealing treatment to achieve the superconducting properties. Beneficial as well as detrimental defects are introduced at this stage. Dislocations, twins, and stacking faults act as pinning centres for magnetic vortices and greatly enhance the material performance. Cracks are also induced by the oxygenation [12]. The a/b-microcracks are formed because the thermal expansion of the Y123 phase in the c-direction is higher than that of the Y211 phase. However, the microcracks are also formed because the c parameter with oxygen uptake decreases [9]. The a/b- and a/c-oxygenation cracks have been shown to be related to the change of the c- and average $(a + b)/2$ parameters due to oxygen uptake [12, 14, 15]. Because of very low diffusion rates, this change takes place over a reduced thickness and yields large stresses leading to an intense regular material cracking. The crack spacing has been shown to depend on the oxygen annealing temperature [15]. If not controlled, the excellent superconducting properties are damaged by the poor mechanical ones. The reduction of crack formation in this material is a crucial issue for applications.

A progressive-oxygenation process has been shown to drastically reduce cracks [12]. However, this treatment can only be applied to samples with thickness smaller than 1.5 mm along the direction parallel to the a/b-planes.

We report in this paper the development of thin-wall single-domain bulk samples suitable for applying this oxygenation strategy. Thin-wall geometry implies a regular network of holes with a fine pitch, e.g. $\varnothing$1 mm holes with 2.4 mm spacing. This network was machined or pressed and single domains up to 4 cm were grown. Some previous works reported the growth of single domains on particular geometries such as cavities [16], foams [17], or shapes using a pre-defined 3D wax model [18]. However, the possibility to obtain a high-quality single domain on such a fine network was not *a priori* obvious. Although this work was developed in the specific context to obtain a/b-crack free samples, we will show that this geometry also provides samples suitable for levitation or trapped-field purpose.

Recently, a record trapped field above 17 T was obtained at 29 K on a 3 cm single-domain sample on which a 1 mm hole was drilled after growth and filled with a low melting point metallic alloy [19]. Because the production of high trapped field [19, 20] and the use of pulse magnetization [21] yield high electromechanical constraints, mechanical reinforcement and thermal stability are important issues for applications. Thin-wall single-domain samples offer a significant potential not only for oxygenation but also for mechanical reinforcement and thermal stability [18, 22].

2. Experimental procedure

2.1. Sample preparation

The pellets used to grow the single-domain samples are prepared from a mixture of commercial powders: 70 wt% of Y123 (SR30 grade from Solvay Barium GmbH with a grain size distributed around 15 μm), 30 wt% of Y211 (solid state powder from SCPI with a grain size varying around 2 μm) and 0.15 wt% representing an excess of PtO_2 (Aldrich). The Y211 insulating phase has a higher melting point than Y123 and so it provides a solid skeleton during melting so that the pellets can keep their shape. It is also source of yttrium during the growth. Moreover, distributed as small particles in the Y123 matrix, it introduces pinning centres when this matrix becomes superconducting.

The platinum addition counteracts Ostwald ripening at high temperature and ensures that the size of the Y211 particles remains small ($\sim$1–2 μm) [23]. The size of the Y211 particle is actually a compromise, as a coarser size of Y211 particles introduces cracks due to the mismatch of the thermal expansion with the Y123 matrix, while a finer size leads to cracks due to the inhomogeneities associated with the pushing–trapping phenomenon at the advancing growth front. The present composition and our process are known to give average but reproducible performances [5]. The thin-wall geometry was obtained either by machining slightly sintered pellets or more recently by compacting pellets with embedded needles.

In the first case, pellets of the mixed precursors are obtained in a $\varnothing$25 mm die under an 80 MPa uniaxial pressure. The weight and height of the pellets are 30 g and 16 mm respectively. Since the green pellets are too brittle for machining, a sintering step at 910 °C during 6 h is performed to insure a moderate, but sufficient, consolidation. At this stage, the pellets can be drilled using commercial HSS (high speed steel) drills coated with a diamond film against abrasion. The standard smallest diameter available being 1 mm, a triangular array of 1 mm diameter holes separated by 2.4 mm is drilled parallel to the pellet axis (see figure 1). The wall thickness of the obtained geometry is less than 1.5 mm. One large $\varnothing$40 mm pellet was also prepared by the same procedure.

In the second case, a 20 mm diameter die was modified to insert 0.7 mm diameter and 7 cm long stainless steel needles. The needles are maintained by the bottom and top pressing plates to form a triangular array of 0.7 mm holes separated by 2.5 mm. The mixed precursors are poured in the die and uniaxially pressed at a moderate pressure of 50 MPa. The needles are removed from the die before releasing the pellet.

The pressing procedure is faster than drilling, and, besides, smaller holes can be achieved on rather large depth (3 cm). But the pressing procedure requires special tools made for each size and geometry to be tested. On the other hand, mechanical drilling is limited in terms of a minimum size achievable and the drilling depth. However, it is more flexible for investigating different types of hole arrays.

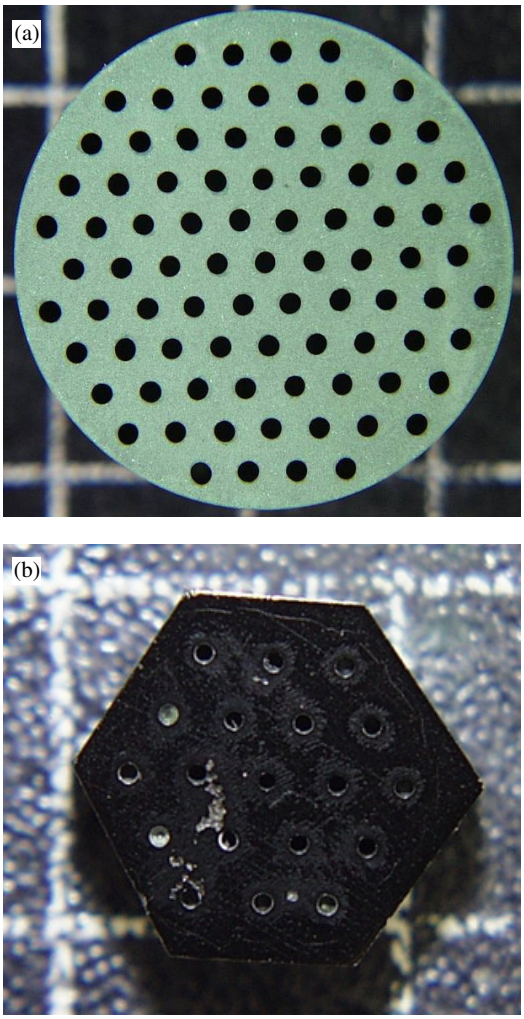

Figure 1. Pictures of a slightly sintered YBCO pellet with a thin-wall geometry after drilling an array of holes (a). A hexagonal sample cut out of a sample pressed with embedded needles (b) (the background grid is on a cm scale).

2.2. Top seeded melt texturing

Thin-wall single-domain samples are prepared following the classical single-domain procedure by the TSMG method. An important point is that the precursor pellet is shaped with the thin-wall geometry before the growth of the single domain. This differentiates the present work from the others where the single domains are machined once grown, as in [19].

The pellets with machined or pressed hole arrays are put in the furnace on an alumina plate with alternate layers such as a buffer of Y_2O_3 powder, to absorb liquid loss and reduce reaction with alumina. An intermediate pressed disc of a mixture of 80 wt% $YBa_2Cu_3O_{7-x}$ and 20 wt% $YbBa_2Cu_3O_{7-x}$ helps to avoid a parasitic nucleation from the pellet bottom by introducing a compound with a lower melting point [5].

The single domains are grown from a $SmBa_2Cu_3O_x$ seed placed between the holes in the centre of the pellet top surface at the beginning of the process. This seed is cut from a $SmBa_2Cu_3O_x$ single domain, the *c*-axis of which is set parallel to the pellet vertical axis.

The pellet is overheated for 2 h in air at 1054 °C. The seed is preserved while the pellet is peritectically decomposed into a liquid rich in barium and copper and a skeleton of solid Y211 particles. The recombination into Y123 and the single-domain growth from the seed then take place around 1000 °C in a narrow solidification range through which the pellet is slowly cooled at the rate of 0.16 °C h^{-1} until the single domain reaches the pellet edge. A subsequent cooling at 0.5–1 °C h^{-1} enables the growth to proceed down to the pellet bottom. The final ramp down to room temperature is performed under flowing nitrogen to prevent the oxygenation *a*/*b*-cracks.

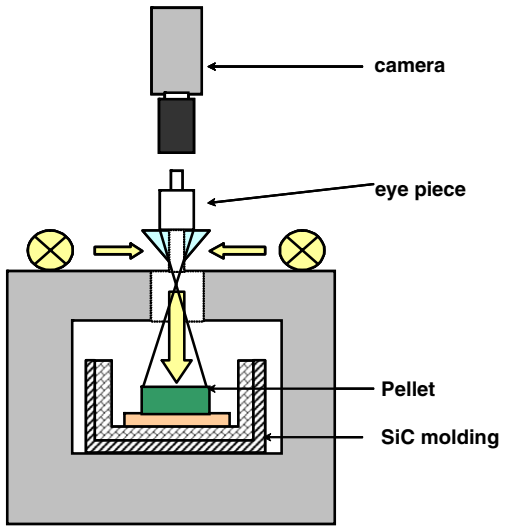

Figure 2. Modified box furnace for video monitoring of surface growth. The contrast is obtained from the reflection of two halogen lights.

The process is carried out in a modified box furnace, shown in figure 2, where the surface is continuously monitored with a video camera [5]. Pictures of the surface are stored every hour on a computer, while the process temperature is recorded every minute. The single-domain growth is evidenced thanks to the surface contrast created by the reflection of two halogen lights. In the present conditions the surface growth-front speed is estimated at 0.3 mm h^{-1}. The useful working range for the growth is no more than 10 °C, but may vary with the powder quality. The information derived from the surface pictures associated with the process temperatures allows the process adjustment.

2.3. Oxygenation

For comparison purposes, a first set of samples (hereafter plain sample and drilled sample) was annealed under flowing oxygen in two steps, first at 420 °C for 144 h, then at 380 °C for 288 h. This kind of oxygenation (hereafter classical oxygenation) yields an intensive cracking of the bulk even in thin-wall samples.

The main reason for introducing thin-wall geometry is to apply a progressive-oxygenation process for crack reduction as proposed in [12]. However, progressive oxygenation at ambient pressure leads to an extremely long process (months) if one has to obtain an oxygen content close to $YBa_2Cu_3O_7$, even for thin-wall single-domain samples. The use of oxygen under high pressure enables one to work at a higher temperature for equivalent final oxygen content in the sample

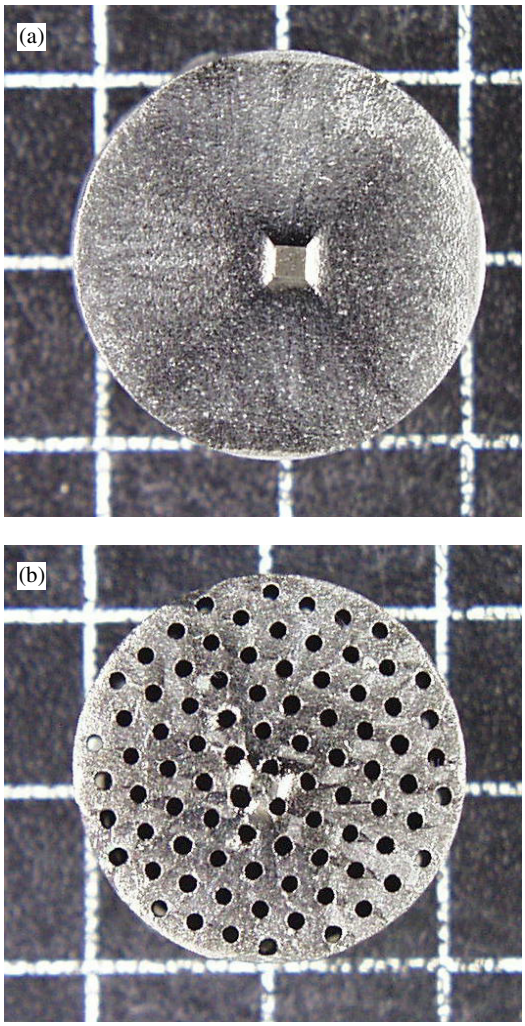

Figure 3. Top surface of a plain pellet (a) and of a drilled one (b). The diagonals characteristic of the squared pattern of the single-domain growth cannot be distinguished anymore on the drilled pellet. Streaks and kinks are visible as the growth front crosses the holes and becomes divided.

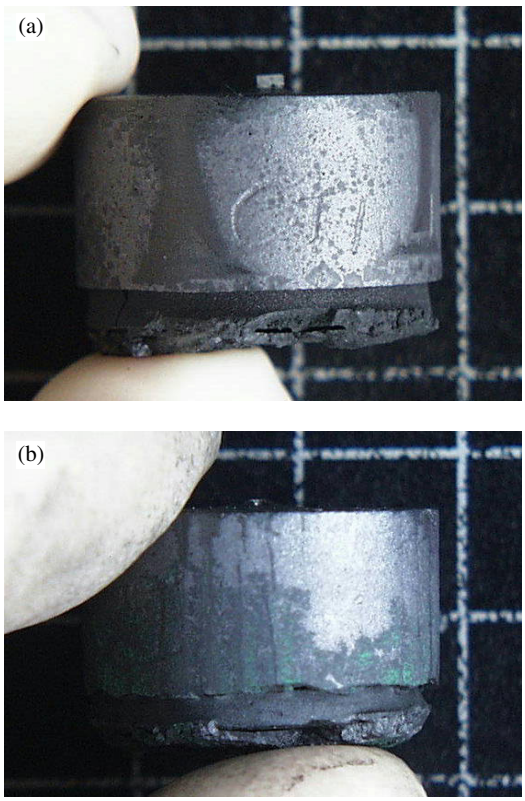

Figure 4. Side view of a plain pellet (a) and of a drilled one (b). Marked lines corresponding to the trace of the single-domain diagonals on the side surface confirm the in-depth growth of the single domain down to the substrate. These lines are multiple in the case of the drilled sample as a result of the growth-front splitting by holes in the diagonal region, i.e. the steps visible at the surface.

(e.g. [13]). The higher the temperature the faster is the diffusion, so that the process can be substantially accelerated.

One sample with a pressed array of holes (hereafter pressed sample) was oxygenated at 160 bar (16 MPa) in a refractory steel vessel. The edges of this sample were cut around the hexagonal central part where the holes are located to keep the thin-wall geometry (see figure 1). A new, gradual oxygenation process was used for this sample. After heating under flowing nitrogen up to 900 °C, the atmosphere of the furnace was changed to 1 bar of oxygen. The temperature was cooled at 10 °C h^{-1} down to 800 °C for a 2 h dwell, then at 4 °C h^{-1} down to 750 °C for another 4 h dwell. Starting at 800 °C, the oxygen pressure was slowly raised up to 30 bar at 5 bar h^{-1}, then up to 160 bar at 10 bar h^{-1}. This progressive increase was used since a direct increase to 160 bar results in the sample breaking into small pieces because of the cracks induced by the oxygen gradient between the surface and the bulk. Subsequent dwells are performed at 700 °C (7 h), 650 °C (12 h), 600 °C (24 h) and 550 °C (44 h) with ramps of 2.5, 1.25, 0.8 and 0.4 °C h^{-1} respectively. At the end of the last dwell, the sample was assumed to be fully oxygenated and was cooled down to room temperature at 60 °C h^{-1}. Oxygen pressure was then released to ambient pressure. The treatment, which still needs to be optimized, was decided upon using the data compiled by Assmus *et al* [24]. Other data [13, 25] tend to show that full oxygenation under pressure above 100 bar may already be achieved around 700 °C.

3. Results and discussion

3.1. Single-domain growth [26]

The top and side surface morphology of a plain sample and of a drilled one can be compared in figures 3 and 4. A single domain with vertical *c*-axis grows on the surface starting from the oriented seed and keeps a square shape with sides parallel to the [100] and [010] directions. This growth habit is recognizable by the diagonals marking the [110] growth-sector boundaries (figure 3(a)). The growth in depth follows the [001] direction and can be checked by the trace of the [110] diagonals along the side surface as the domain reaches the edge (figure 4(a)).

The final morphology is different for a single domain grown on a drilled pellet. It is difficult to recognize the single-domain features described above in figure 3(b). Streaks

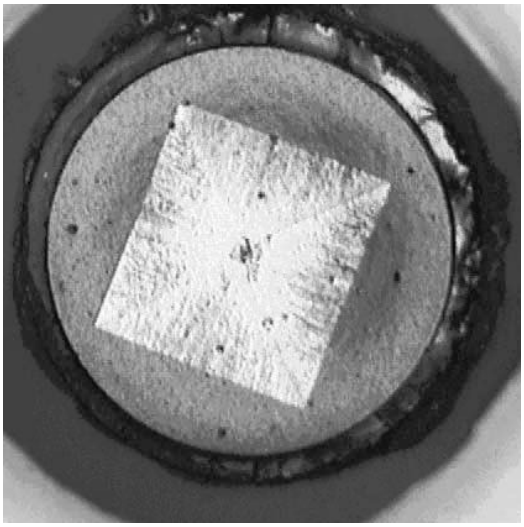

Figure 5. Growth of a single domain on a ⌀50 mm plain pellet. The crystal growth at the surface is seen as a square since the YBCO tetragonal phase is growing on the surface along the *a*- and *b*-directions imposed by the seed located at the centre. Video 1 of the growth is available at stacks.iop.org/SUST/19/S590.

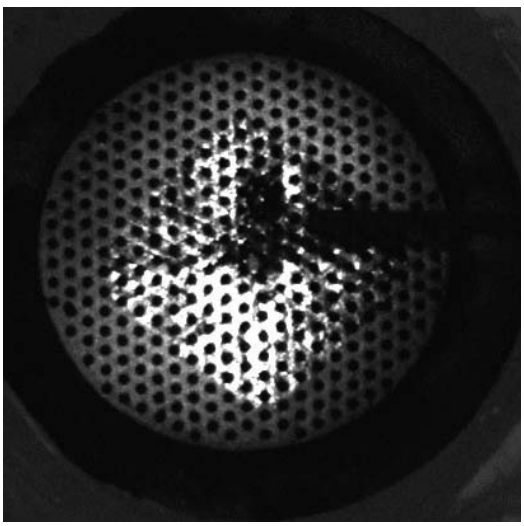

Figure 6. Growth of a single domain on a ⌀50 mm drilled pellet. The growth fronts are deflected by the holes, which yield kinks and streaks. The growing crystal does not appear any longer as a square with clear diagonals, making it difficult to ascertain after the growth the single-domain nature. Video 2 of the growth is available at stacks.iop.org/SUST/19/S590.

and steps can be noticed behind the holes, indicating an interaction between the growth front and the hole network. On the side surface, the vertical black lines associated with the intersection of the [110] diagonals with the edge become multiple thin lines.

In situ video during the growth help to clarify the growth process. Figure 5 shows an intermediate growth stage on a ⌀50 mm plain pellet. The square pattern associated with the growth habit in the [100] and [010] directions can be seen in the middle of the picture, the first circle around being the edge of the pellet. For the growth on a ⌀50 mm drilled pellet, figure 6 shows a similar process but slightly distorted by the hole array.

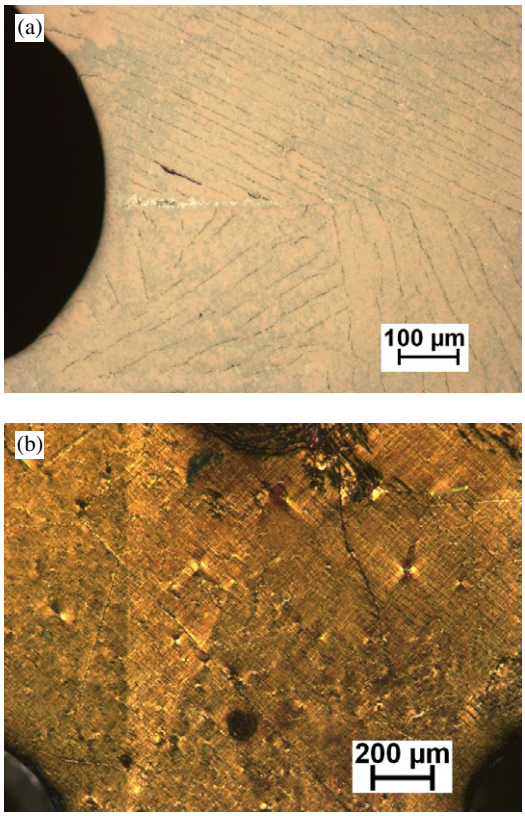

Figure 7. Pictures of the surroundings of a hole. (a) A secondary phase trace (white line on the right of the hole) marks the line where the *a*-growth subsectors meet behind the hole in the growth direction. (b) A lighter area can be seen below the upper hole. This area is Y211 particles depleted compared to the rest of the surface.

The effect of a hole is to divide the growth front into two parts that will merge behind the hole in two possible ways.

If the hole is far from the growing-square corners, the two resulting growth fronts continue to grow symmetrically and then join eventually somewhere behind the hole, leaving sometimes a small streak between the growth-front junction and the hole. The streaks correspond to a Y211 depleted area or locally trapped secondary phases (see figure 7).

If the hole is near a corner of the growing single domain, the growth front is divided into two advancing corners, which later join, making a kink. As a result of this corner subdivision, the growing single domain does not appear any longer as a net square, the edge being rounded by the creation of multiple kinks (see figure 6).

The sample shown in figure 6 is still a single domain as confirmed by quantitative texture analysis using neutron diffraction [28] on samples of 1 cm^2 taken from the bulk. The experiment was conducted at the D1B beamline facility of the Institut Laue Langevin at Grenoble, France. Figure 8 shows the resulting {100} and {003} pole figures. Only one domain orientation appears using a 5°-step scanning grid. Despite the surface defects mentioned above, no significant misorientation is introduced in the bulk.

3.2. Microstructure

3.2.1. Single-domain continuity. The microstructure was checked on polished surfaces with a polarized optical

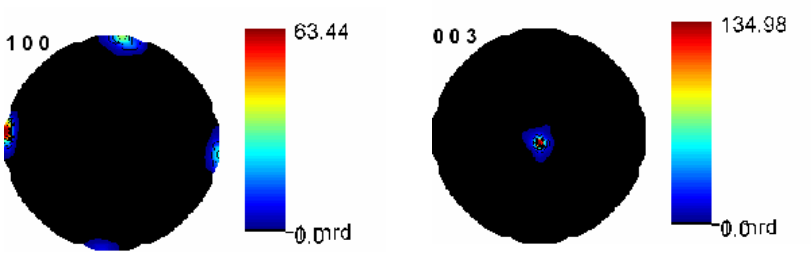

Figure 8. Quantitative texture analysis using neutron diffraction on a cubic cm size sample taken from a ⌀50 mm drilled pellet. Only one bulk orientation appears in the {100} and {003} pole figures.

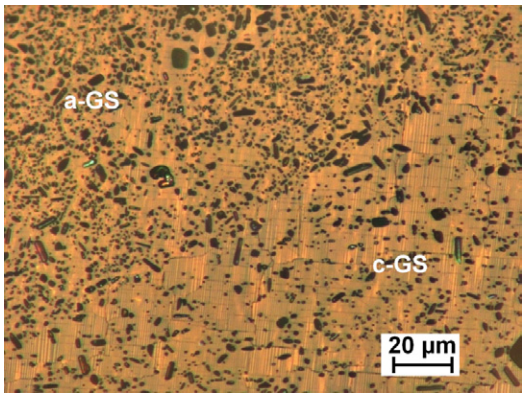

Figure 9. Picture in polarized light of an a/c-section of a drilled oxygenated pellet. The bottom right part (c-growth sector) is Y211 depleted due to the pushing–trapping phenomenon. Microcracks along the a/b-planes are visible. GS stands for growth sector.

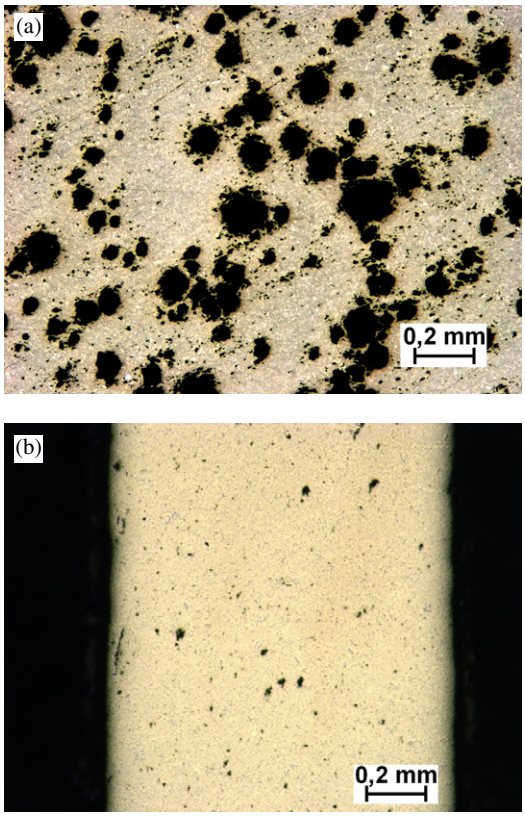

Figure 10. Pictures in polarized light of an a/c-section of a plain pellet (a) and of a drilled one (b). These samples were cooled under nitrogen and are not oxygenated. The striking difference is a drastic reduction of the porosity in the drilled pellet. Note the absence of macrocracks.

microscope. The growth of a single domain on drilled pellets is confirmed by the continuity of the twinning pattern and the absence of an orientation change. The microstructure is similar in plain, drilled, and pressed samples, i.e. the same distribution of Y211 particles in the Y123 matrix. The same subgrain structure can be observed in polarized light on vertical cuts of each sample type: elongated c-axis subgrains below the seed in the c-growth sector and elongated a- or b-axis subgrains close to the edge in the a- or b-growth sectors. The pyramid imprint due to the difference of the pushing–trapping effect between c-growth and a- or b-growth sectors is also present in drilled samples, as can be seen in figure 9.

The most striking difference is a drastic reduction of porosity in drilled samples, as can be seen in figure 10. In plain samples, a 2–3 mm dense layer without porosity is seen on the surface, but a distribution of pores around 100 μm is then always found in the bulk. In contrast, no pores are visible in single-domain samples grown on drilled or pressed pellets. This is typical of a thin-wall geometry with a hole spacing below 4 mm. The reduced diffusion path intended to improve the oxygenation is also helpful during the domain formation to release trapped gas, i.e. oxygen lost during melting [6, 29, 30].

3.2.2. Cracks. Holes by themselves are not sufficient to avoid cracking. At each stage, caution should be taken to avoid any crack formation. Since stresses are concentrated at crack tips [31], any macrocracks already existing will tend to develop on further oxygenation and deteriorate the sample. It is noteworthy to observe in figure 10 the absence of macrocracks in samples that have been cooled from 950 °C to room temperature under a nitrogen flow to avoid oxygen uptake during cooling. In contrast, figure 11 gives an example of regular macrocracking that occurs at the surfaces of a drilled sample without oxygen annealing but just cooled under air after the domain growth.

Figure 12 presents pictures of the top surface (a/b-plane) of oxygenated samples taken at low magnification under polarized light. Figure 12(a) represents a plain sample where an a/c-oxygenation crack network can be observed (right side of the picture). For some reasons, a thin layer with a thickness of about 1 mm located in the centre area of the surface pellet remains in the tetragonal phase (see grey left

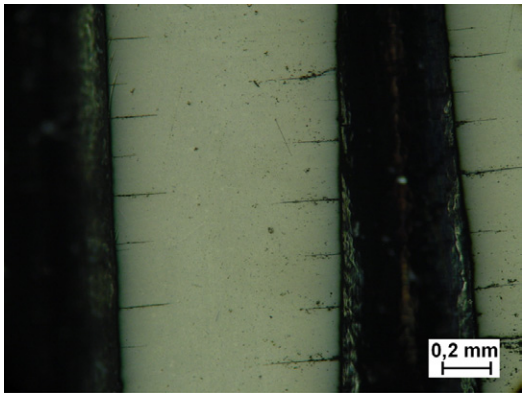

Figure 11. Regular macrocracks due to oxygen uptake at high temperature on a sample cooled under air.

area of the picture) despite an oxygenation time of 432 h; this non-oxygenated phase is crack free. The persistence of a tetragonal layer has also been reported in the case of a two-step oxygenation process by Kracunovska *et al* [32]. The orthorhombic phase is characterized by a two-colour contrast, orange and dark green, which in fact each represents a twinning set with main directions perpendicular to each other. Figures 12(b) and (c) are from a drilled sample (with 1 mm drilled holes) and a pressed one (with 0.7 mm pressed holes), respectively. The holes do not appear deformed by the growth process, but their dimension has been reduced by 20% during the bulk densification (sintering and melting). The 1 and 0.7 mm diameters are reduced to 0.8 and 0.56 mm, respectively. The whole surface is oxygenated and the same two-colour contrast associated with the twin complex pattern is observed as for the plain pellet. However, the colours are not uniformly distributed around the holes, but well separated, which is an indication of a stress field [27]. Depending on the stress direction, one twinning direction is privileged over the other. A starting macrocrack can be observed at the hole bottom edge (figure 12(b)) and seems aligned along the twin pattern. In the case of the smaller hole (pressed sample, progressively oxygenated under pressure, figure 12(c)), the stress field seems to be attenuated (the twin complex pattern looks more uniform), which may support the idea that smaller holes and/or progressive oxygenation are preferable. In both cases, the presence of holes is associated with the absence of a/c-oxygenation cracks, which would be beneficial to flux trapping or levitation.

All observed cracks are parallel to the cleavage planes of the Y123 phase, which means that they are formed on the already grown single-domain sample. As expected, despite the holes, the classical oxygenation yields an intensive a/b-plane macrocracking as can be seen in figure 13. For comparison, a view of one a/c-side of the pressed sample oxygenated under pressure is shown in figure 14. Both macrographs were obtained at the same magnification using a stereo microscope. On the latter, one main macrocrack can be seen in the middle with its border decomposed into small grains during the temperature ramp to 900 °C under nitrogen. This is an indication that this crack was already present before the oxygenation. The other cracks are a/b-oxygenation cracks. A very positive and encouraging point is that they are in a much

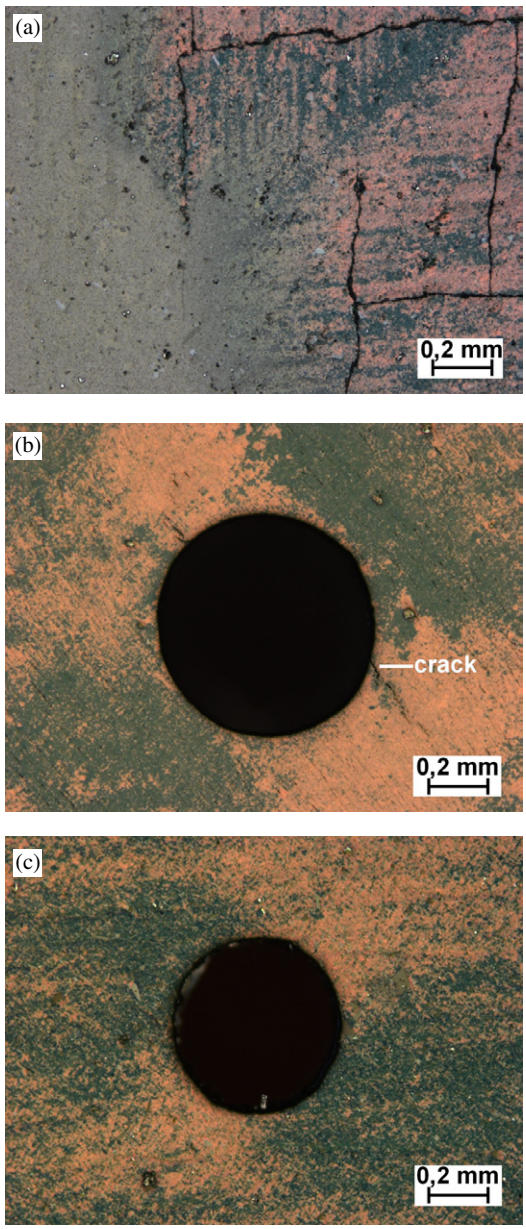

Figure 12. Surface of a plain sample after classical oxygenation (a). The grey area on the left remained in the tetragonal phase. The orthorhombic area is characterized by a network of a/c-oxygenation cracks. The contrast inside the area is due to a twin complex pattern, each colour representing a main perpendicular direction of twinning. Surfaces around a hole in a drilled sample (b) and in a pressed one (c). The size of the hole is 0.8 mm for the drilled sample and 0.56 mm for the pressed sample. Note the absence of a/c-cracks and the non-uniform distribution of the twin complex pattern indicating the presence of a stress field. A crack aligned with the pattern started from the bottom edge of the hole in the drilled sample (b). The stress field seems to be attenuated in the pressed sample (c) since the distribution pattern is less contrasted.

reduced number when compared to a sample after a classical oxygenation (figure 13) and that no a/c-oxygenation cracks are found.

It should be noted that no radial cracks were found around the holes, contrary to [27], indicating that these reported radial cracks are linked to some processing difference.

Figure 13. Macrograph using a stereo microscope of an a/c-section taken from a drilled sample (thickness ∼6 mm) with a classical oxygenation characterized by an intensive cracking along the a/b-planes.

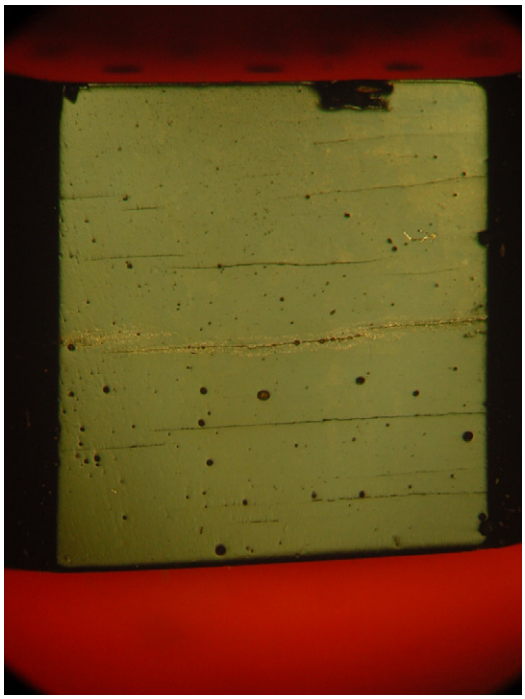

Figure 14. Macrograph using a stereo microscope of an a/c-face of a pressed sample oxygenated under pressure (thickness ∼6 mm).

3.3. Flux trapping

As compared to local transport or magnetic J_c measurements on small samples extracted from the bulk, the flux trapping provides more complete information on the quality of the whole sample, because it takes into account the superconducting current loop size.

The remnant induction at the surface of the samples has been measured after a magnetization cycle with a Hall probe. The scan is performed at 77 K at a distance of 0.2 mm of the surface with a grid step of 0.5 mm. By taking into account the time needed to ramp the field down and to place the sample onto the scanning set-up, the measurement is made more than 20 min after magnetization, so that relaxation phenomenon can be neglected during the experiment. This experimental set-up yields results which are within a few per cent of those obtained in other European laboratories (round robin test led by Cardwell *et al* [33]).

Figure 15 shows the results obtained on a plain and a drilled sample with classical oxygenation (144 h at 420 °C, 288 h at 380 °C) after being field-cooled in 2 T. The 2D representation of the magnetic flux isocurves follows a squared contour for the plain sample matching the square pattern of the single-domain growth. This contour is more rounded for the drilled sample and reflects the smoothing of the growth front passing through the hole network. To reveal the hole network, a complementary technique, e.g. magneto-scan [34], has to be used. The holes themselves cannot be distinguished in remnant flux profiles, but some indentations can be noticed, for example, on the top part of the contour lines that could be ascribed to the presence of holes. In both cases, the current loops circulate on the sample scale.

3.3.1. Drilled sample. Remarkably, in the drilled sample the maximum remnant trapped field (532 mT) is higher by 40% than in the plain sample (375 mT), despite the fact that the bulk volume decreases by 18% by the hole presence. Considering just a hole network in a bulk with a constant quality of material (i.e. constant J_c), drilled samples would always have lower performances than plain samples because of a reduction in effective area. The only way to diminish this influence would be to reduce as much as possible the hole diameter [35]. The influence of the hole size has been confirmed in [34]. In the present case, it clearly appears that the material quality is well enhanced. Obvious factors are the matrix densification and the reduction of a/c-oxygenation cracks (in these samples the a/b-cracking remains intensive, as seen in figure 13).

It was also observed, using SQUID measurement on $5 \times 5 \times 5$ mm^3 cubic samples classically oxygenated, that drilled samples are better oxygenated with the sharpest transition (figure 16) and show higher magnetization at 88 K. Measurements at a lower temperature were not possible due to the saturation of the apparatus. An effective macroscopic critical current density is determined from the measured magnetization, applying the standard critical state model, i.e. $J_c = 3 \times \Delta M/d$ in SI units, where d is the sample diameter. The hole influence is taken into account by using a factor related to the superconducting-to-total area ratio [35]. This ratio is about 0.85 for the drilled sample. According to the data in [35], the factor to be used is 0.70 and the local critical current density is the macroscopic critical current divided by this factor. The critical current densities are plotted in figure 17 for both plain and drilled samples. The critical current density of the drilled sample is higher than the one of the plain sample, thus confirming the material improvement in a thin-wall geometry.

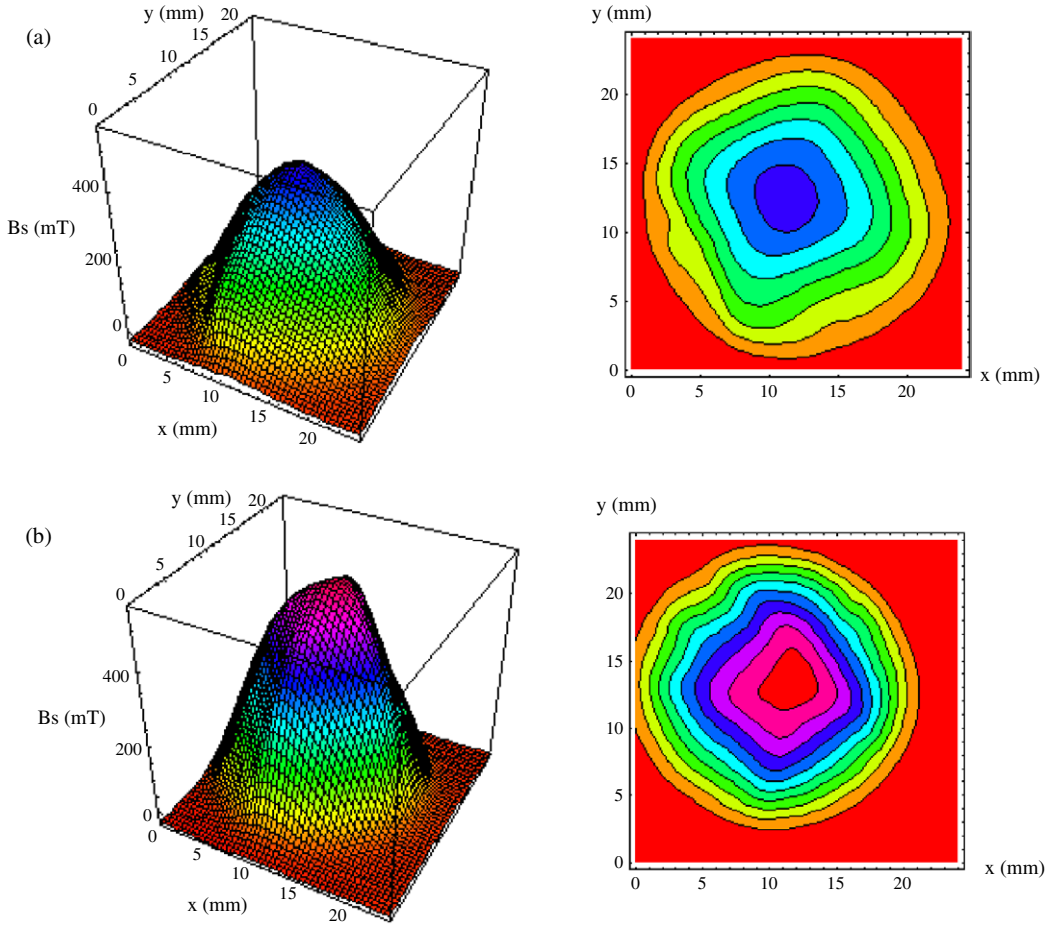

Figure 15. Comparison of flux mapping after field cooling at 2 T and 77 K on a plain sample (a) and a drilled sample (b), both 22 mm in diameter. The trapped field is higher in the drilled sample (532 mT) than in the plain one (375 mT).

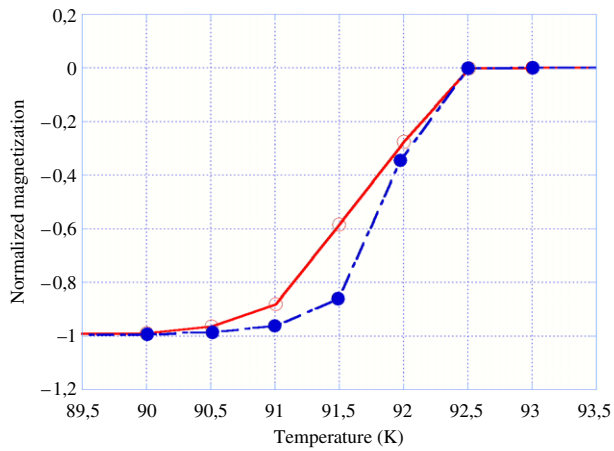

Figure 16. Magnetization versus temperature curves of $5 \times 5 \times 5$ mm^3 cubic samples, one plain (open circles) and one drilled (plain circles), after a classical oxygenation. A sharper transition indicates that the drilled sample is better oxygenated than the plain one.

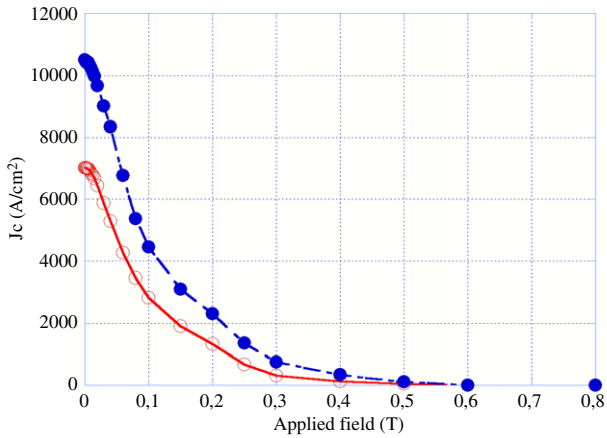

Figure 17. Calculated J_c from magnetization data at 88 K of $5 \times 5 \times 5$ mm^3 cubic samples, one plain (open circles) and one drilled (plain circles), after a classical oxygenation. The J_c is higher in the drilled sample as a result of a better material quality and oxygenation.

3.3.2. Pressed sample. Figure 18 shows the remnant flux profiles obtained on a hexagonal pressed sample progressively oxygenated under pressure. Whereas in the previous samples the magnetic flux isocurves were following the single-domain boundary, in this case they are following the sample contour as it was cut in the grown single domain. The maximum

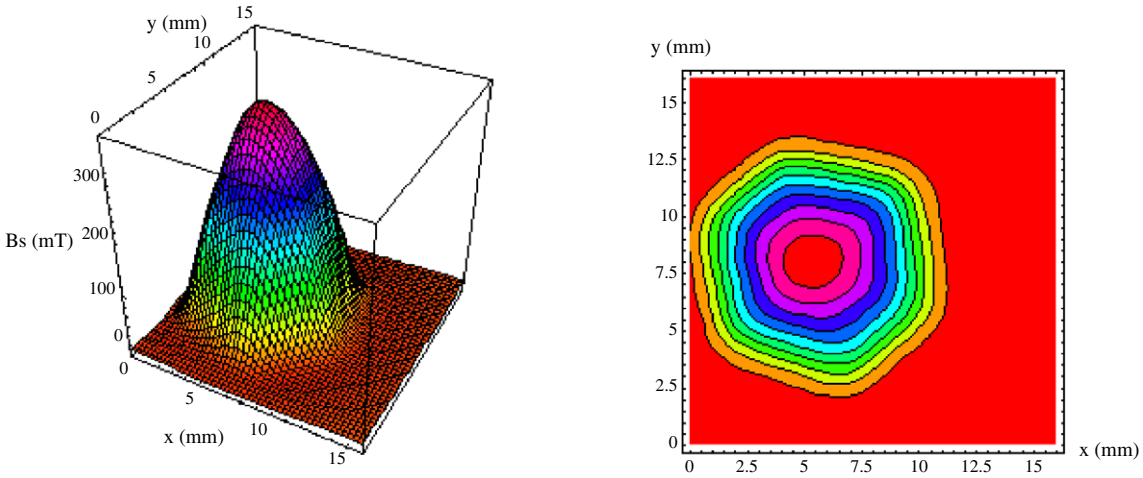

Figure 18. Flux map on a hexagonal pressed sample progressively oxygenated under pressure (10 mm inscribed diameter). The maximum remnant trapped field is 336 mT.

remnant trapped field is 336 mT for current loops included in a 10 mm diameter circle. Assuming that the material quality would remain unchanged for a larger pellet and that the proportionality with the sample diameter would be maintained, an improvement of 25% is achieved compared to the previous sample (670 mT versus 532 mT) and the trapped field would attain 1 T for a 30 mm pellet at 77 K.

These results validate the use of the pressing method to obtain the thin-wall geometry although the improvement has to be confirmed on larger samples. It is not clear at present whether this could be attributed to the hole smaller size or to the progressive oxygenation.

4. Conclusions

Thin-wall geometry was obtained by drilling holes in slightly sintered pellets or by pressing the pellets with embedded needles. The growth of a single-domain sample up to a 50 mm diameter on such thin-wall geometry pellets was confirmed by *in situ* high-temperature video monitoring. The presence of holes influences the growth front and some surface defects are introduced. However, it was established by various techniques (neutron diffraction pattern, microstructure analysis, flux mapping) that the bulk is a single domain.

The microstructures of plain and thin-wall samples are similar in terms of distribution of secondary phase and subgrains, but a clear difference exists in terms of porosities and cracks. The reduction of diffusion paths attained by thin-wall geometry enables the gas, especially oxygen, which is released during melting and which is at the origin of pores, to escape out of the sample. For both drilled and pressed samples, the cracks formed along the c-axis are reduced in number. The improvement of the material quality is established by a significant increase of about 40% of the trapped field in the thin-wall samples, whereas the presence of holes decreases the superconducting volume by 18%. A cracking reduction in a/b-planes is observed and may be related to a 25% enhancement of the trapped field in the pressed sample. Further experiments are needed to confirm the beneficial effect of progressive oxygenation on flux-trapping capabilities.

Since more spectacular improvement of the trapped field have been shown in recent experiments using improved compositions, for instance GdBaCuO compounds [7], it is of interest to check whether the observed enhancement related to thin-wall geometry can be reproduced for such composition.

Finally, it should be noted that with the present composition thin-wall geometry is not only beneficial for flux trapping, but also provides a material ready for further practical improvements such as mechanical reinforcement and thermal stabilization.

Acknowledgments

The authors would like to thank the EFFORT network (http://www.rebco-effort.org) for providing an encouraging environment to pursue the development of bulk REBaCuO single-domain samples, the PASREG committee for the motivating invitation to the Tokyo meeting and the CNRS for providing a position which allowed P Diko to come to the CRETA group. Finally, P Diko would like to thank the VEGA foundation and NANOSMART for financial support.

References

[1] Schochlin A, Ritter T and Bornemann H J 1995 *IEEE Trans. Magn.* **31** 4217
[2] Tixador P *et al* 2000 *Supercond. Sci. Technol.* **13** 493
[3] Ren Y, Liu J, Weinstein R, Chen I G, Parks D, Xu J, Obot V and Foster C 1993 *J. Appl. Phys.* **74** 718
[4] Matsuzaki H, Kimura Y, Ohtani I, Izumi M, Ida T, Akita Y, Sugimoto H, Miki M and Kitano M 2005 *IEEE Trans. Appl. Supercond.* **15** 2222
[5] Isfort D, Chaud X, Beaugnon E, Bourgault D and Tournier R 2000 *Inst. Phys. Conf. Ser.* vol. 167 (Bristol: Institute of Physics Publishing) p 47
[6] Sakai N, Inoue K, Nariki S, Hu A, Murakami M and Hirabayashi I 2005 *Physica* C **426–431** 515
[7] Muralidhar M, Sakai N, Jirsa M, Murakami M and Koshizuka N 2005 *Supercond. Sci. Technol.* **18** L9
[8] Nariki S, Sakai N and Murakami M 2002 *Supercond. Sci. Technol.* **15** 648

[9] Diko P 2004 *Supercond. Sci. Technol.* **17** R45
[10] Kingery W D, Bowen H K and Uhlmann D R 1976 *Introduction to Ceramics* (New York: Wiley) p 820
[11] Tournier R F, Isfort D, Bourgault D, Chaud X, Buzon D, Floch E, Porcar L and Tixador P 2003 *Physica* C **386** 467
[12] Isfort D, Chaud X, Tournier R and Kapelski G 2003 *Physica* C **390** 341
[13] Wang J, Monot I, Chaud X, Erraud A, Marinel S, Delamare M P, Provost J and Desgardin G 1998 *Physica* C **304** 191
[14] Specht E D, Sparks C J, Dhere A G, Brynestad J, Cavin O B, Kroeger D M and Oye H A 1988 *Phys. Rev.* B **37** 7426
[15] Diko P and Krabbes G 2003 *Supercond. Sci. Technol.* **16** 90
[16] Pandit H *et al* 2005 *Physica* C **425** 44
[17] Reddy E S and Schmitz G J 2002 *Supercond. Sci. Technol.* **15** L21
[18] Sudhakar Reddy E, Hari Babu N, Shi Y, Cardwell D A and Schmitz G J 2005 *Supercond. Sci. Technol.* **18** S15
[19] Tomita M and Murakami M 2003 *Nature* **421** 517
[20] Krabbes G, Fuchs G, Verges P, Diko P, Stöver G and Gruss S 2002 *Physica* C **378–381** 636
[21] Yanagi Y, Itoh Y, Yoshikawa M, Oka T, Ikuta H and Mizutani U 2005 *Supercond. Sci. Technol.* **18** 839
[22] Laurent Ph, Matthieu J P, Mattivi B, Fagnard J F, Meslin S, Noudem J G, Ausloos M, Cloots R and Vanderbemden Ph 2005 *Supercond. Sci. Technol.* **18** 1047
[23] Ogawa N, Hirabayashi I and Tanaka S 1991 *Physica* C **177** 101
[24] Assmus W and Schmidbauer W 1993 *Supercond. Sci. Technol.* **6** 555
[25] Prikhna *et al* 2004 *Supercond. Sci. Technol.* **17** S515–9
[26] Chaud X, Meslin S, Noudem J, Harnois C, Porcar L, Chateigner D and Tournier R 2005 *J. Cryst. Growth* **275** e855–e860
Chaud X, Isfort D, Porcar L and Tournier R 2005 *J. Eur. Ceram. Soc.* **25** 2955
[27] Diko P, Kračunovská S, Ceniga L, Zeisberger M and Gawalek W 2005 *Supercond. Sci. Technol.* **18** 1400
[28] Chateigner D, Ricote J, Chaud X, Gautier-Picard P, Beaugnon E, Soubeyroux J L, Leblond C and Monot I 1999 *ICOTOM XII: Textures of Materials* ed J A Szpunar (Ottawa: NRC Research Press) p 457
[29] Krabbes G, Bieger W, Wiesner U, Ritschel M, Hauck J and Altenburg H 1991 *Physica* C **185–189** 503
[30] Chaud X, Beaugnon E, Derango P, Ducloux F, Tournier R, Hiebel P, Tixador P and Brunet Y 1994 *Physica* C **235–240** 433
[31] Kanninen M F and Popelar C H 1985 *Advanced Fracture Mechanics* (New York: Oxford University Press)
[32] Kračunovská S, Diko P, Litzkendorf D, Habisreuther T, Bierlich J and Gawalek W 2005 *Supercond. Sci. Technol.* **18** S142
[33] Cardwell D A *et al* 2004 *Physica* C **412–414** 623
[34] Haindl S, Hengstberger F, Weber H W, Meslin S, Noudem J and Chaud X 2006 *Supercond. Sci. Technol.* **19** 108
[35] Bartolomé E, Granados X, Puig T, Obradors X, Reddy E S and Kracunovska S 2005 *IEEE Trans. Appl. Supercond.* **15** 2775–8